Progress In Electromagnetics Research Letters, Vol. 113, 7–15, 2023

Facile Synthesis, Kinetics and Photocatalytic Study of Ultrasmall Aluminum Nanoparticles

Hao Wu[1, 2], Rongrong Zhu[1], Sichao Du[1], Hao Xie[1], and Jun Hu[2, *]

Abstract—Ultrasmall nanoparticles with tunable photo-optical properties and colloidal nature are ideal for a wide range of photocatalytic reaction. Herein, we reported the facile synthesis of ultrasmall aluminum nanoparticles (AlNPs), which exhibited unique UV-B photoluminescence and excitation wavelength dependent fluorescence characteristic. Spherical aberration-corrected scanning transmission electron microscope (ACTEM) and X-ray photoelectron spectroscopy (XPS) were used to study the microstructure and verify the successful synthesis of AlNPs. Time-resolved photoluminescence spectroscopy was employed to gain insight into the unique photoluminescence behavior. The photocatalytic activity of ultrasmall AlNPs was evaluated by the photoreduction of resazurin (RZ) to resorufin (RF) under UV light irradiation. This photodegradation of RZ obeyed the pseudo-first-order reaction kinetics with reaction rate achieved $6.62 \times 10^{-2}\,\mathrm{min}^{-1}$. Our study suggested that the prepared ultrasmall AlNPs have a great potential application in photocatalytic field.

1. INTRODUCTION

Ultrasmall metal nanoparticles in sub-3-nm usually exhibits molecular properties, such as HOMO-LUMO transitions [1], bright photoluminescence (PL) [2], large Stoke shift [3], chirality [4], magnetism [5] due to the electrons of metal atoms confined in molecular dimensions. These typical molecular features make ultrasmall metal nanoparticles suitable for metal iron detection [6], nanocatalysts [7], bioimaging [8], photothermal therapy [9], etc. In the last two decades, ultrasmall metal nanoparticles have been widely used in catalysis research owing to the unique atom-stacking way and enriched catalytic active sites [10]. Especially for spherical particles, a substantial reduction in particles size leads to a dramatic increase in surface area, which gives rise to the specific photocatalytic activities. However, researchers mainly focus on the noble metals (such as Au, Ag, Cu, Pt) for their reactivity and catalytic properties [11, 12]. In view of economy and experimental feasibility, it is valuable to seek other inexpensive and earth-abundant metal catalysts as a replacement.

Due to the unique plasmonic properties extending to the ultraviolet region and its abundant earth reserves, aluminum has attracted extensive attention from researchers [13]. However, there are still many important challenges preventing people from conducting extensive research on it, such as reliable fabrication of aluminum instead of expensive nanosphere lithography (NSL) or e-beam lithography (EBL) method [14] and excessive oxidation of small-sized aluminum nanoparticles [15]. Herein, a facile, environmentally friendly and cost effective reverse micellar method was reported to realize the successful synthesis of ultrasmall aluminum nanoparticles (AlNPs). The morphology, structural, and metallic state characteristics of AlNPs were studied using spherical aberration-corrected scanning transmission electron microscope (ACTEM) and X-ray photoelectron spectroscopy (XPS).

Received 18 September 2023, Accepted 30 September 2023, Scheduled 12 October 2023

* Corresponding author: Rongrong Zhu (rorozhu@zucc.edu.cn).

[1] School of Information and Electrical Engineering, Hangzhou City University, Hangzhou 310015, China. [2] ZJU-JITRI Joint R&D Center of Applied Spectroscopy Technologies, College of Optical Science and Engineering, Zhejiang University, Hangzhou 310058, China.

The photophysical properties were studied through UV-Vis spectroscopy, steady-state and time-resolved photoluminescence study. In order to further confirm the feasibility of AlNPs as a nanocatalyst, a redox indicator resazurin (RZ) was used to evaluate the photocatalytic properties. To our knowledge, this is the first report on the photocatalytic properties of ultrasmall AlNPs.

2. MATERIALS AND METHODS

2.1. Materials

Aluminum chloride ($AlCl_3$, anhydrous, powder, 99.999%), Tetraoctylammonium bromide (TOAB, 98%) and lithium aluminum hydride ($LiAlH_4$, 2.4 M solution in THF) were obtained from Sigma Aldrich. Resazurin (RZ), Tetradecylphosphonic Acid (TDPA, > 98%), xylene (anhydrous, > 98%), Dimethylformamide (DMF, 99.5%) were purchased from Aladdin Corp. Dry ethanol (99.7%) was purchased from Sinopharm Chemical Reagent Co., Ltd. All solvents were distilled to remove oxygen and water prior to use.

2.2. Methods

All glassware used in the study were fully dried (130° for 8 h) before experiment. All experiments were performed under an insert atmosphere using standard Schlenk Line filled with argon. The ultra-small aluminum nanoparticles were synthesized in reverse micelles by the solution-phase reduction of $AlCl_3$ with $LiAlH_4$ in anhydrous xylene. Surface modification of the ultra-small aluminum nanoparticles was achieved by treating the surface of the particles with TDPA. Ultrasmall AlNPs studied in this research were prepared using a modified method reported by our previous study [16]. 133 mg $AlCl_3$ (1 mmol) was dissolved into 2 mmol/L TOAB xylene solution for the purpose of purification. A reducing agent with a molar ratio of 2 : 1 was added, and the solution was stirred for one hour, producing unmodified AlQDs. The surface modification followed the previous experimental protocol.

2.3. Characterization

Field Emission Transmission Electron Microscopy (Tecnai G^2F20 S-TWIN FEI) was used to study the morphology and size distribution of ultrasmall AlNPs. Spherical Aberration Corrected Field Emission Transmission Electron Microscope (Titan $G^2$60-300 FEI) operated at 300 kV was used to observe the atom alignments and study the lattice morphologis. The X-ray photoelectron spectroscopy (XPS, Thermo ESCALAB XI^+, Thermo Fisher Scientific) with Al Kα radiation as the excitation source was used to verify the successful synthesis and study the metallic state of ultrsmall AlNPs. UV-Vis scanning spectrometer (UV2550, Shimadzu, Japan) and fluorescence spectrometer (F2500, Hitachi, Japan) with Xenon lamp excitation were used to record the optical response of ultrasmall AlNPs.

2.4. Photocatalytic Experiment

The photocatalytic experiment was carried out as follows: adding different amounts of AlNPs (2.5 mg, 2 mg, 1.5 mg, 1 mg) into 10 ml solution of 4.5 μg/ml RZ. Before starting the photocatalytic experiments, the mixed solution was thoroughly stirred to ensure the adsorption-desorption equilibrium for 20 min in the dark condition. Use 200 mw 405 nm laser diode to irradiate the reaction vessel to initiate the photocatalytic process. The UV-Vis spectra were recorded every two minutes to monitor the process.

3. RESULTS AND DISCUSSION

The morphologies of the as-prepared ultrasmall AlNPs were analyzed by high-resolution transition electron microscopy (HRTEM) and ACTEM. The observed AlNPs were monodispersed and exhibited a nice spherical shape as shown in Figure 1(a). The average diameter of AlNPs was 3.70 ± 0.43 nm as shown in Figure 1(b). To further verify the successful synthesis of ultrasmall AlNPs, ACTEM was employed to investigate the microstructure, as shown in Figure 1(c). As discussed by Douglas-Gallardo et al., the icosahedral is the most stable structure for aluminum under 5 nm [17], which perfectly matched with our

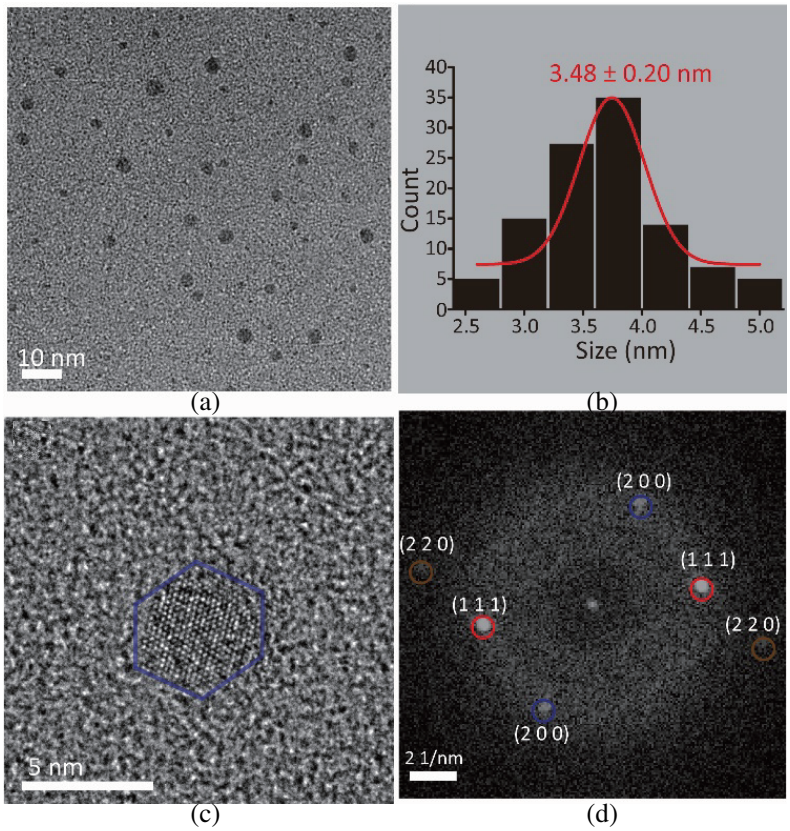

Figure 1. (a) HRTEM image of synthesized AlNPs; (b) the size distribution analysis of synthesized AlNPs; (c) an ACTEM image of an individual aluminum nanoparticles; (d) the corresponding Fast Fourier Transformation of the AlNPs.

experimental results. In addition, the corresponding fast Fourier Transformation of single aluminum nanoparticle was recorded in Figure 1(d). The lattice spacings of obtained nanocrystals were measured to be 0.23 nm, 0.20 nm, and 0.14 nm, which could be assigned to the (111), (200), and (220) facets of aluminum, respectively. The angle between (111) and (200) facets was $\sim 54°$, and the angle between (200) and (220) facets was about 90° matched with face-centered cubic structure. It was worth noting that point defects on the surface of AlNPs were expected to provide a large number of active sites for photocatalysis. The above results revealed the characteristic of single-crystal phase and suggested the successful synthesis of ultrasmall aluminum nanoparticles.

The surface composition and chemical states of related elements were analyzed by X-ray photoelectron spectroscopy (XPS). The XPS spectra were corrected by the carbon peak of 284.6 eV. The full scan spectrum revealed the existence of carbon (C1s 284.6 eV), nitrogen (N1s 398.4 eV), and aluminum (Al2p 73.1 eV) as shown in Figure 2(a). It was worth noting that aluminum had a low oxidation resistance, which naturally created a 2–3 nm thick alumina passivation layer. Considering the ultrasmall size of AlNPs, on the one hand, the presence of aluminum oxide would greatly affect its photoluminescence performance; on the other hand, it would hinder the transport of electrons on its surface. The high-resolution spectra of Al 2p showed one main peak at 73.1 eV, which was consistent with the previous study [15]. It could be clearly seen that there was no peak at 75.7 eV belonging to aluminum oxide, indicating that the oxidation issue could be significantly inhibited by the reverse micellar liquid phase synthesis method.

The distinct optical behaviour of as-prepared AlNPs was recorded by UV-Vis absorption and photoluminescence spectroscope techniques (as shown in Figure 3). The formation of ultrasmall AlNPs exhibited the characteristic adsorption peak around 260 nm, due to the plasma resonance excitation

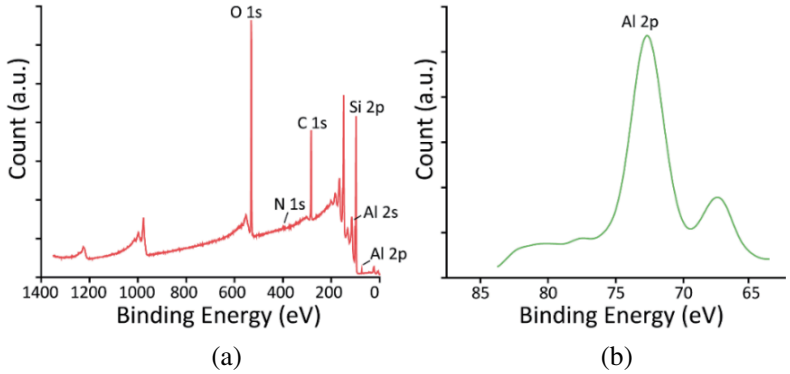

Figure 2. XPS survey scan of ultrasmall AlNPs spin-coated on silicon wafer. (a) XPS full scan spectrum; (b) high resolution survey scan of Al 2p region.

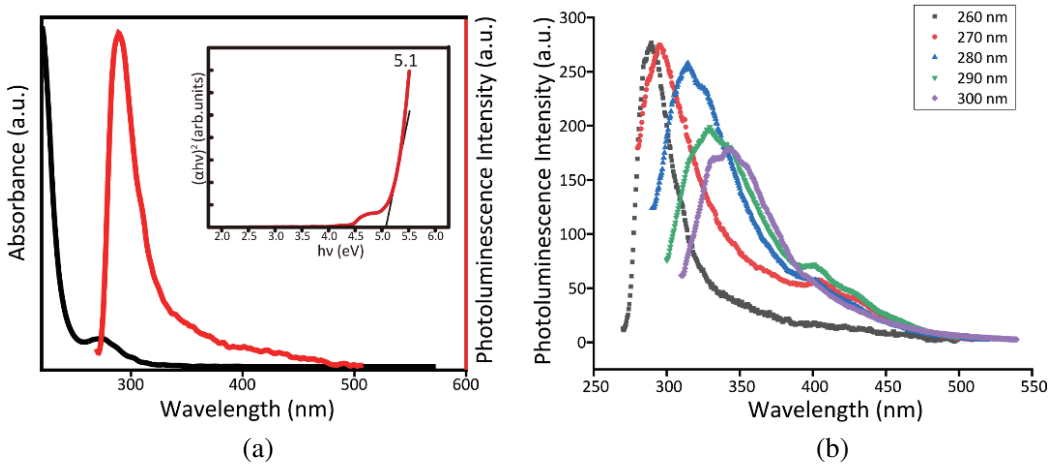

Figure 3. (a) UV-Vis absorption spectrum and photoluminescence spectrum (λ_{ex}–260 nm), the inset picture showed the Tauc plot of AlNPs sample; (b) Excited wavelength dependent emission spectra of AlNPs ranging between 260 nm–300 nm, respectively.

of Al atoms on the surface of nanoparticles. The effective band gaps of ultrasmall AlNPs could be deduced to about 5.1 eV, through Tauc plot method [18]. Meanwhile, the steady photoluminescence was recorded in Figure 3(a), which exhibited UV-B fluorescence under 260 nm excitation.

We next focused on the steady photoluminescence behavior of AlNPs. The as-prepared sample exhibited strong UV-B photoluminescence with an emission peak at 300 nm excited by 260 nm. Generally, when the size of nanoparticle becomes comparable to the electron Fermi wavelength of corresponding metal, the continuous band structure breaks into discrete energy states [19], thus making them behave like molecules. The excitation wavelength dependent emission spectra were recorded in Figure 3(b). It could be clearly seen that the fluorescence spectra gradually red-shifted with broadening spectra and decreased intensity, when the excitation source was changed from 260 nm to 310 nm. The Kasha's rule explained that for organic dyes and inorganic semiconductors, the excited electrons relaxation process is independent of the excitation wavelength [20]. However, inhomogeneous broadening of the fluorescence spectrum was observed in our experimental results when the elicitation wavelength was changed. For small noble metal nanoclusters, the surface states have been considered as the reason for the broad and excitation-dependent photoluminescence behavior [21–23]. This might be ascribed to the solvation process, where the ethanol solvent dipole would rotate to rearrange in a comparable energy level with the excited-state dipole of AlNPs, thus lowering the energy of the excited states [24].

To further investigated the effect of surface ligands on the relaxation kinetics of AlNPs, the Fourier Transform Infrared Spectrometer (FTIR) was used to characterized the surface group composition as shown in Figure 4. The peak located at 760 cm^{-1} represented Al-N transverse optical phonon mode [25] and 1450 cm^{-1} for C-N mode [26, 27], which indicated the adsorption behavior of TOAB. The peak located around 3400 cm^{-1} attributed to the O-H stretching mode, which might be introduced by the H_2O from the atmosphere. The peak located at 1152 cm^{-1} was the stretching vibration of $P = O$, and the 1356 cm^{-1} was the bending vibration of P-O [28, 29], which indicated the successful modification of TDPA.

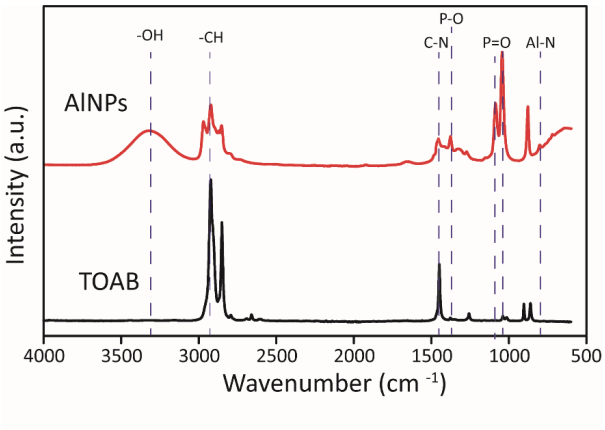

Figure 4. FTIR spectra of synthesized ultrasmall AlNPs and used surfactant template TOAB.

To explore the charge carrier relaxation dynamics of AlNPs, time-resolved photoluminescence studies were performed. The fluorescence decay trace was recorded in Figure 5, and could be fitted with double exponential decay function. The fitting parameters were shown in the inset table of Figure 5. We anticipated that the 700 ps component were mainly attributed to the radiative recombination related to the core state; While, the longer 3.9 ns lifetime component was originated from the surface state related to the absorbed TOAB and TDPA, which has been reported by several researchers [30, 31].

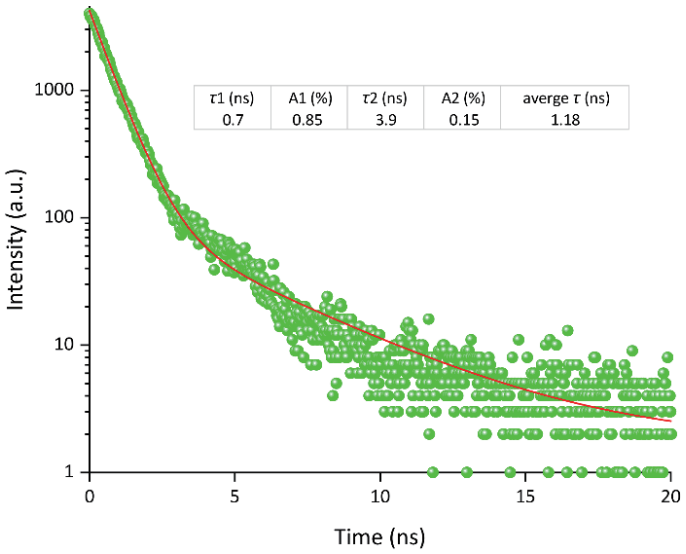

Figure 5. Fluorescence decay trace of ultrasmall AlNPs (excited at 280 nm and collected at 310 nm).

Ultrasmall AlNPs could maximize the external area of aluminum nanoparticles, and the surface defects could serve as active sites. Hence, the photocatalytic activity of AlNPs was evaluated by the photoreduction of RZ under UV irradiation (400 nm). RZ is a blue colored redox-indicator with

a maximum absorbance at 610 nm and can be reduced into RF (a pink color dye with maximum absorbance at 578 nm) [32]. By adding different amounts of AlNPs (2.5 mg, 2 mg, 1.5 mg, 1 mg) into the RZ solution with the same concentration, the changes of the absorption spectra were recorded every two minutes. Figure 6(a) shows the absorption spectra change of the experimental group with 2 mg AlNPs added. It could be clearly seen that the characteristic absorption peak of RZ (640 nm) was gradually decreased under the UV irradiation, along with the gradual rise of the characteristic absorption peak of RF (578 nm). The inset pictures were the experimental group, control group, andthe blank control group. Under UV light irradiation and the presence of AlNP, the RZ solution changed from blue to pink, indicating that RZ was photocatalytically reduced to RF. However, if the RZ solution was only irradiated with UV light, the color of the solution became lighter, indicating that RZ was only photodegraded. Figure 6(b) shows the control experimental results, where the RZ solution was only irradiated with UV light at regular intervals.

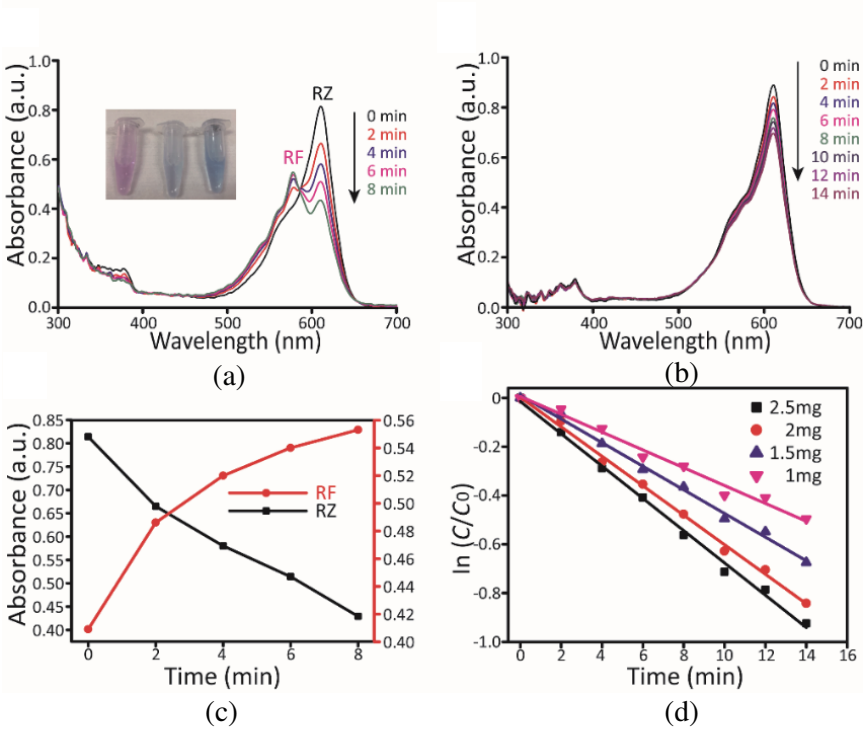

Figure 6. (a) Time dependent reduction of RZ into RF catalyzed by AlNPs. Inset: Photographic of AlNPs-RZ mixture after irradiation (left), RZ solution after irradiation (middle), AlNPs-RZ mixture without irradiation. (b) Time dependent reduction of RZ without adding AlNPs as photocatalyst. (c) Corresponding absorbance intensity change of RZ (610 nm) and RF (578 nm) under different reaction time. (d). Fitting plot of reaction kinetics using different AlNPs photocatalyst concentrations.

In order to intuitively demonstrate the process of photocatalytic reduction of RZ to RF by AlNPs under UV irradiation, Figure 6(c) recorded the intensity evolution of corresponding characteristic absorption peak. It could be seen that the photodegradation and photocatalytic reduction processes of RZ occurred simultaneously during the whole experiment. By fitting the intensity change of 610 nm absorption peak of four experimental groups, it was found that the photodegradation of RZ followed the pseudo-first-order reaction, which can be described as $(\mathrm{In}C_t/C_0) = -kt$. Through using the characteristic adsorption peak intensity at 0 min to represent C_0 and the corresponding peak intensity after t minutes of reaction for C_t, the fitting curves were recorded in Figure 6(d). The resulting slope was the apparent rate constant k for the photodegradation reaction. In our case, the values of k for AlNPs with concentration 2.5, 2.0, 1.5, 1 mg were found to be 6.62×10^{-2}, 6.05×10^{-2}, 4.85×10^{-2}, $3.66 \times 10^{-2}\,\mathrm{min}^{-1}$, which were much larger than previous studies [13, 14].

The mechanism for the photocatalytic reaction involved several steps. Firstly, the UV light was

absorbed by both AlNPs and dye molecule. Due to the quantum confinement effect of ultrasmall AlNPs and surface plasmonic resonance (SPR) resonance of relatively large nanoparticles, irradiated AlNPs absorbed the photons ($h\nu$) then generated an electron-hole pair ($e^-_{CB}+h^+_{VB}$) and enriched electron density on the surface. The photocatalytic reduction process mainly involved the RZ molecule absorbed electrons on the surface of AlNPs leading to the cleavage of N-O, along with the color of the solution changed from blue into pink. This was verified by the results in Figure 6(a), with the decreased intensity in 380 nm which was the characteristic n-π^* transition of the N-oxide of the RZ molecule [33].

4. CONCLUSION

In summary, we reported the successful synthesis of ultrasmall AlNPs ($\sim$ 3.5 nm) through reverse micellar method, which showed highly-efficient photocatalysis properties. The ACTEM results suggested the synthesized AlNPs exhibited good crystallinity with low point defect concentration. The XPS study revealed that the oxidation issue of aluminum could be solved through organic liquid phase synthesis method. Then we studied the physiochemical properties of AlNPs, which exhibited excellent UV-B photoluminescence and excitation wavelength dependent photoluminescence. FTIR and time-resolved photoluminescence studies were conducted to study the surface composition and surface-state emission behavior of ultrasmall AlNPs. Moreover, the photocatalytic activity of ultrasmall AlNPs was firstly observed and evaluated by the photoreduction of RZ into RF under UV irradiation, which obeyed the pseudo-first-order kinetics. The photoexcited electrons of AlNPs due to the quantum confinement effect and SPR effect were absorbed by the RZ molecule, thus triggering the photocatalytic degradation process, which was verified by our experimental results. In a word, we have shown that ultrasmall AlNPs could find use as a low-cost, earth-abundant, and potential harmless photocatalyst, and opens an avenue for the construction of photocatalysts with aluminum based composite structures.

ACKNOWLEDGMENT

This work was sponsored by the Natural Science Foundation of Zhejiang Province under Grant No. LQ21F050002.

REFERENCES

1. Zhu, M., C. M. Aikens, F. J. Hollander, G. C. Schatz, and R. Jin, "Correlating the crystal structure of a thiol-protected Au25 cluster and optical properties," *Journal of the American Chemical Society*, Vol. 130, No. 18, 5883–5885, May 1, 2008, doi: 10.1021/ja801173r.
2. Duan, H. and S. Nie, "Etching colloidal gold nanocrystals with hyperbranched and multivalent polymers: A new route to fluorescent and water-soluble atomic clusters," *Journal of the American Chemical Society*, Vol. 129, No. 9, 2412–2413, Mar. 1, 2007, doi: 10.1021/ja067727t.
3. Zhou, C., G. Hao, P. Thomas, J. Liu, M. Yu, S. Sun, O. K. Öz, X. Sun, and J. Zheng, "Near-infrared emitting radioactive gold nanoparticles with molecular pharmacokinetics," *Angewandte Chemie International Edition*, Vol. 51, No. 40, 10118–10122, Oct. 1, 2012.
4. Zeng, C., T. Li, A. Das, N. L. Rosi, and R. Jin, "Chiral structure of thiolate-protected 28-gold-atom nanocluster determined by X-ray crystallography," *Journal of the American Chemical Society*, Vol. 135, No. 27, 10011–10013, Jul. 10, 2013, doi: 10.1021/ja404058q.
5. Kim, B. H., N. Lee, H. Kim, K. An, Y. I. Park, Y. Choi, K. Shin, Y. Lee, S. G. Kwon, H. B. Na, J.-G. Park, T.-Y. Ahn, Y.-W. Kim, W. K. Moon, S. H. Choi, and T. Hyeon, "Large-scale synthesis of uniform and extremely small-sized iron oxide nanoparticles for high-resolution T1 magnetic resonance imaging contrast agents," *Journal of the American Chemical Society*, Vol. 133, No. 32, 12624–12631, Aug. 17, 2011, doi: 10.1021/ja203340u.
6. Shellaiah, M., K. Awasthi, S. Chandran, B. Aazaad, K. W. Sun, N. Ohta, S.-P. Wu, and M.-C. Lin, "Methylammonium tin tribromide quantum dots for heavy metal ion detection and cellular imaging," *ACS Applied Nano Materials*, Vol. 5, No. 2, 2859–2874, Feb. 25, 2022, doi: 10.1021/acsanm.2c00028.

7. Wang, N., Q. Sun, and J. Yu, "Ultrasmall metal nanoparticles confined within crystalline nanoporous materials: A fascinating class of nanocatalysts," *Advanced Materials*, Vol. 31, No. 1, 1803966, Jan. 1, 2019.
8. Liu, Z., Z. Wu, Q. Yao, Y. Cao, O. J. H. Chai, and J. Xie, "Correlations between the fundamentals and applications of ultrasmall metal nanoclusters: Recent advances in catalysis and biomedical applications," *Nano Today*, Vol. 36, 101053, Feb. 1, 2021, doi: 10.1016/j.nantod.2020.101053.
9. Ma, Z., Y. Zhang, J. Zhang, W. Zhang, M. F. Foda, X. Dai, and H. Han, "Ultrasmall peptide-coated platinum nanoparticles for precise NIR-II photothermal therapy by mitochondrial targeting," *ACS Applied Materials & Interfaces*, Vol. 12, No. 35, 39434–39443, Sep. 2, 2020, doi: 10.1021/acsami.0c11469.
10. Jin, R., C. Zeng, M. Zhou, and Y. Chen, "Atomically precise colloidal metal nanoclusters and nanoparticles: Fundamentals and opportunities," *Chemical Reviews*, Vol. 116, No. 18, 10346–10413, Sep. 28, 2016, doi: 10.1021/acs.chemrev.5b00703.
11. Liang, H., B.-J. Liu, B. Tang, S.-C. Zhu, S. Li, X.-Z. Ge, J.-L. Li, J.-R. Zhu, and F.-X. Xiao, "Atomically precise metal nanocluster-mediated photocatalysis," *ACS Catalysis*, Vol. 12, No. 7, 4216–4226, Apr. 1, 2022, doi: 10.1021/acscatal.2c00841.
12. Kawawaki, T., Y. Kataoka, M. Hirata, Y. Akinaga, R. Takahata, K. Wakamatsu, Y. Fujiki, M. Kataoka, S. Kikkawa, A. S. Alotabi, S. Hossain, D. J. Osborn, T. Teranishi, G. G. Andersson, G. F. Metha, S. Yamazoe, and Y. Negishi, "Creation of high-performance heterogeneous photocatalysts by controlling ligand desorption and particle size of gold nanocluster," *Angewandte Chemie International Edition*, Vol. 60, No. 39, 21340–21350, Sep. 20, 2021, doi: 10.1002/anie.202104911.
13. Christopher, P., H. Xin, A. Marimuthu, and S. Linic, "Singular characteristics and unique chemical bond activation mechanisms of photocatalytic reactions on plasmonic nanostructures," *Nature Materials*, Vol. 11, No. 12, 1044–1050, Dec. 1, 2012, doi: 10.1038/nmat3454.
14. Honda, M., Y. Kumamoto, A. Taguchi, Y. Saito, and S. Kawata, "Plasmon-enhanced UV photocatalysis," *Applied Physics Letters*, Vol. 104, No. 6, 2014, doi: 10.1063/1.4864395.
15. Knight, M. W., N. S. King, L. Liu, H. O. Everitt, P. Nordlander, and N. J. Halas, "Aluminum for plasmonics," *ACS Nano*, Vol. 8, No. 1, 834–840, Jan. 28, 2014, doi: 10.1021/nn405495q.
16. Wu, H., X. Cheng, S. Xie, Y. Huang, R. A. Janjua, X. Liu, and S. He, "Aluminum quantum dots with surface controlled blue-UV photoluminescence," *The Journal of Physical Chemistry C*, Vol. 127, No. 5, 2687–2693, Feb. 9, 2023, doi: 10.1021/acs.jpcc.2c08441.
17. Douglas-Gallardo, O. A., G. J. Soldano, M. M. Mariscal, and C. G. Snchez, "Effects of oxidation on the plasmonic properties of aluminum nanoclusters," *Nanoscale*, Vol. 9, No. 44, 17471–17480, 2017, doi: 10.1039/C7NR04904H.
18. Makuła, P., M. Pacia, and W. Macyk, "How to correctly determine the band gap energy of modified semiconductor photocatalysts based on UV-Vis spectra," *The Journal of Physical Chemistry Letters*, Vol. 9, No. 23, 6814–6817, Dec. 6, 2018, doi: 10.1021/acs.jpclett.8b02892.
19. Schaaff, T. G., G. Knight, M. N. Shafigullin, R. F. Borkman, and R. L. Whetten, "Isolation and selected properties of a 10.4 kDa Gold: Glutathione cluster compound," *The Journal of Physical Chemistry B*, Vol. 102, No. 52, 10643–10646, Dec. 1, 1998, doi: 10.1021/jp9830528.
20. Kasha, M., "Characterization of electronic transitions in complex molecules," *Discussions of the Faraday Society*, Vol. 9, No. 0, 14–19, 10.1039/DF9500900014, 1950, doi: 10.1039/DF9500900014.
21. Díez, I., R. H. A. Ras, M. I. Kanyuk, and A. P. Demchenko, "On heterogeneity in fluorescent few-atom silver nanoclusters," *Physical Chemistry Chemical Physics*, Vol. 15, No. 3, 979–985, 2013, doi: 10.1039/C2CP43045B.
22. Zhou, M., e, S. Long, X. Wan, Y. Li, Y. Niu, Q. Guo, Q.-M. Wang, and A. Xia, "Ultrafast relaxation dynamics of phosphine-protected, rod-shaped Au20 clusters: interplay between solvation and surface trapping," *Physical Chemistry Chemical Physics*, Vol. 16, No. 34, 18288–18293, 2014, doi: 10.1039/C4CP02336F.

23. Wen, X., P. Yu, Y.-R. Toh, X. Ma, S. Huang, and J. Tang, "Fluorescence origin and spectral broadening mechanism in atomically precise Au8 nanoclusters," *Nanoscale*, Vol. 5, No. 21, 10251–10257, 2013, doi: 10.1039/C3NR03015F.
24. Zhou, M. and R. Jin, "Optical properties and excited-state dynamics of atomically precise gold nanoclusters," *Annual Review of Physical Chemistry*, Vol. 72, No. 1, 121–142, Apr. 20, 2021, doi: 10.1146/annurev-physchem-090419-104921.
25. Ning, J., et al., "Synthesis and structural properties of AlCNO composite thin films," *Thin Solid Films*, Vol. 385, No. 1, 55–60, Apr. 2, 2001, doi: 10.1016/S0040-6090(00)01923-4.
26. Ricci, M., M. Trinquecoste, F. Auguste, R. Canet, P. Delhaes, C. Guimon, G. Pfister-Guillouzo, B. Nysten, and J. P. Issi, "Relationship between the structural organization and the physical properties of PECVD nitrogenated carbons," *Journal of Materials Research*, Vol. 8, No. 3, 480–488, Mar. 1, 1993, doi: 10.1557/JMR.1993.0480.
27. Liu, Z., X. Jing, S. Zhang, and Y. Tian, "A copper nanocluster-based fluorescent probe for real-time imaging and ratiometric biosensing of calcium ions in neurons," *Analytical Chemistry*, Vol. 91, No. 3, 2488–2497, Feb. 5, 2019, doi: 10.1021/acs.analchem.8b05360.
28. Panayotov, D. A. and J. R. Morris, "Thermal decomposition of a chemical warfare agent simulant (DMMP) on TiO_2: Adsorbate reactions with lattice oxygen as studied by infrared spectroscopy," *The Journal of Physical Chemistry C*, Vol. 113, No. 35, 15684–15691, Sep. 3, 2009, doi: 10.1021/jp9036233.
29. Abuelela, A. M., T. A. Mohamed, and O. V. Prezhdo, "DFT simulation and vibrational analysis of the ir and raman spectra of a CdSe quantum dot capped by methylamine and trimethylphosphine oxide ligands," *The Journal of Physical Chemistry C*, Vol. 116, No. 27, 14674–14681, Jul. 12, 2012, doi: 10.1021/jp303275v.
30. Koninti, R. K., S. Satpathi, and P. Hazra, "Ultrafast fluorescence dynamics of highly stable copper nanoclusters synthesized inside the aqueous nanopool of reverse micelles," *The Journal of Physical Chemistry C*, Vol. 122, No. 10, 5742–5752, Mar. 15, 2018, doi: 10.1021/acs.jpcc.7b11457.
31. Zhou, M. and Y. Song, "Origins of visible and near-infrared emissions in [Au25(SR)18]- nanoclusters," *The Journal of Physical Chemistry Letters*, Vol. 12, No. 5, 1514–1519, Feb. 11, 2021, doi: 10.1021/acs.jpclett.1c00120.
32. Mills, A., J. Johnston, and C. O'Rourke, "Photocatalyst activity indicator inks, paiis, for assessing self-cleaning films," *Accounts of Materials Research*, Vol. 3, No. 1, 67–77, Jan. 28, 2022, doi: 10.1021/accountsmr.1c00196.
33. Krishnamoorthy, K., R. Mohan, and S. J. Kim, "Graphene oxide as a photocatalytic material," *Applied Physics Letters*, Vol. 98, No. 24, 244101, 2011, doi: 10.1063/1.3599453.